Powder Technology 407 (2022) 117519

Contents lists available at ScienceDirect

Powder Technology

journal homepage: www.elsevier.com/locate/powtec

Towards a unified theory of wet agglomeration

William Kennedy Walls *, James A. Thompson, Stephen G.R. Brown

Swansea University, Fabian Way, Swansea SA1 8EN, Wales, United Kingdom

ARTICLE INFO

Article history:
Received 7 October 2021
Received in revised form 9 May 2022
Accepted 11 May 2022
Available online 17 May 2022

Keywords:
Granulation
Agglomeration
Growth regime map
Consolidation
Pelletisation
Theoretical model

ABSTRACT

Size control in granulation is of great importance yet is often difficult to achieve. While numerical and analytical models have previously been reported there is still no comprehensive model to describe wet agglomeration systems. In this paper the basis for a new analytical solution towards predict limiting granule size is suggested. The focus of the model is on bulk behaviour of the granules where the interactions in the granular bulk after the initial contact between agglomerating granules continues to affect the properties, such as in high-shear granulation as well as flow processes such as pan or drum agglomeration. The model as developed assumes that granule size is limited by both saturation and dynamic interactions, and matches the results in the literature regarding the final and continuous growth behaviour in those systems where the model is appropriate. Based on the factors that limit the size, granule growth behaviour can be predicted as a consequence of consolidation. The model matches the behaviour of systems captured by classical growth regime maps in a more quantitative manner, and should allow improved scaling as the model develops.

1. Introduction

Wet agglomeration is one of a variety of methods of product size modification, in which a dry powder feed is combined with a binder and then agitated to bind the particles together into granules. Wet agglomeration has been a challenging research area for many years because of its many interconnecting factors and the difficulty of direct experimental observation of the underlying phenomena. Being able to control this process to achieve a target granule size based solely on raw process parameters and material properties would be ideal. However, simply understanding how different parameters interact would be advantageous.

Iveson et al [1] produced a longstanding review that describes many of the factors involved. The problem, as described, is that as a multiphase interaction, agglomeration or pelletization is affected by the properties of the solids, the binder, and the interfaces between them and how the granulation device applies forces to the feed. Furthermore, as Mort [2] discusses, scaling of the process has historically been difficult. The process parameters that are most important can be difficult to directly measure, they can interact in unpredictable ways and are often in direct competition. As an example, when increasing a mixer diameter one cannot keep both the Froude number and the tip speed constant [2]. One way to better manage granulation processes is using regime maps. These map out the different mechanisms occurring as conditions are changed [3].

Fig. 1(a) shows the qualitative growth regime map initially proposed by Iveson and Litster based on the general trends that are observed in practise and is shown alongside Fig. 1(b), where the experimental conditions are noted along with the growth type, to compare the two. Various growth cases from the map have been described elsewhere in the literature, such as steady [5] and induction growth [5–7], with other forms of growth being noted in the literature [8] not mentioned on the map including, equilibrium growth [9,10] and layering [11–13]. The map uses two key parameters to define growth behaviour: saturation and deformation number. This is consistent with reported findings for saturation [5,6,14–16] and kinetics limiting the growth [10,17]. It has also been shown how an increase in the viscosity and reduction in particle size improves the granulation capability of materials, and both parameters contribute to strength [18]. The effect of the distribution of granules on growth has also been reported [19]. When examining mechanism maps quantitatively, the boundaries become less clear and sometimes reported data from other experiments does not fit into the expected regions. Part of this is due to experimental limitations. Unrecognised changes over the process can lead to misrepresented growth patterns, a changing temperature during processing can reduce the viscosity of the material, or in one reported case, release moisture due to hemihydrate decomposition [20], both of which would affect

* Corresponding author.
E-mail address: willkwalls@outlook.com (W.K. Walls).

https://doi.org/10.1016/j.powtec.2022.117519

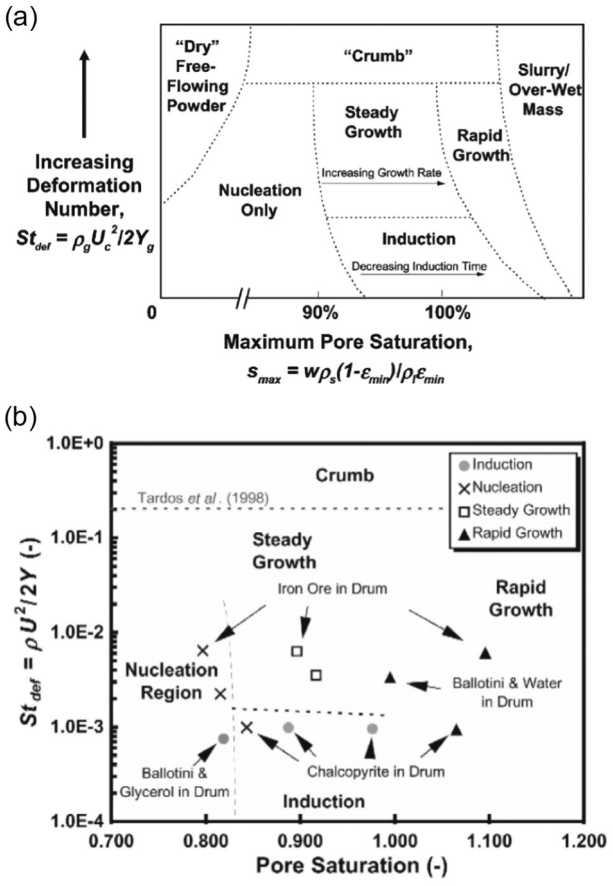

Fig. 1. Granulation regime mapping results by Iveson et al.
(a) The qualitative growth regime map from [4], used with permission of the publisher, indicating the various regimes and how they relate to the deformation number and the maximum pore saturation. (b) From [4], used with permission of the publisher, the qualitative growth behaviour and the saturation/deformation positions of various experiments to validate the map.

the granulation behaviour. Alternatively, the moisture content has been shown in different experiments to reduce over the course of the granulation process [21]. Furthermore, growth regime maps are largely qualitative. Four of the regions usually described, crumb, slurry, dry powder, and nuclei represent steady state situations. In contrast, rapid growth and steady growth regions are rate controlled processes, and induction is a variable rate process. Some work to quantify the boundaries between these regions has been attempted [22] but analytical models could help to determine whether these boundaries are really fixed as the growth regime map implies. The need for a clearly defined analytical solution is also driven by the need for a method that can be implemented efficiently in a discrete element model. Being able to determine for any given collision whether consolidation occurs based on current properties would allow better resource usage due to not needing to record the history of any given granule, and as such a deterministic, memoryless solution is of significant value for such an implementation.

1.1. Analytical models

One well-known model that accounts for both saturation and deformation is here referred to as the Stokes number criterion, which was developed by Ennis et al. [23] and subsequently extended by Liu et al. [24]. This model works to understand the process by dividing up the behaviour into three steps, nucleation, growth, and breakage, subsequently focussing purely on growth behaviour as a function of viscous dissipation. This focus on growth means that it has been used in population balance models as the kernel for growth [25]. While the authors recognise their model is not predictive, they claim it is more meaningful and more physically based compared to kernels obtained by trial and error. Nonetheless it still requires fitting parameters.

1.1.1. Stokes number criterion model

The physically based coalescence model found in [25] comes in three equations, depending on the case at hand, with (1) being "elastic & surface wet", (2) being "plastic & surface wet", and (3) being "plastic & surface dry".

$$\mathrm{St}_v < \left(1+\frac{1}{e_{\mathrm{rest}}}\right)\ln\left(\frac{h_0}{h_a}\right) \tag{1}$$

$$\left(\frac{\sigma_y}{E}\right)^{\frac{1}{2}}(\mathrm{St}_{\mathrm{def}})^{-\frac{9}{8}} < \frac{0.172}{\mathrm{St}_v}\left(\frac{\tilde{D}}{h_0}\right)^2\left[1-\frac{1}{\mathrm{St}_v}\ln\left(\frac{h_0}{h_a}\right)\right]^{\frac{5}{4}} \cdot \times\left[\left(\frac{h_0^2}{h_a^2}-1\right)+\frac{2h_0}{\delta''}\left(\frac{h_0}{h_a}-1\right)+\frac{2h_0^2}{\delta''}\ln\left(\frac{h_0}{h_a}\right)\right] \times\left[1-7.36\left(\frac{\sigma_y}{E}\right)(\mathrm{St}_{\mathrm{def}})^{-\frac{1}{4}}\left(1-\frac{1}{\mathrm{St}_v}\ln\left(\frac{h_0}{h_a}\right)\right)^{-\frac{1}{2}}\right]^2 \tag{2}$$

$$\left(\frac{\sigma_y}{E}\right)^{\frac{1}{2}}(\mathrm{St}_{\mathrm{def}})^{-\frac{9}{8}} < \frac{0.172}{\mathrm{St}_v}\left(\frac{\tilde{D}}{h_0}\right)^2 \cdot \times\left[1-7.36\left(\frac{\sigma_y}{E}\right)(\mathrm{St}_{\mathrm{def}})^{-\frac{1}{4}}\left(1-\frac{1}{\mathrm{St}_v}\ln\left(\frac{h_0}{h_a}\right)\right)^{-\frac{1}{2}}\right]^2 \tag{3}$$

Though the model is intended to account for the various cases of observed granulation phenomena, specifically induction, steady growth and rapid growth, it has not been demonstrated to produce significant predictive results. The liquid surface layer used and the presence of $\mathrm{St}_{\mathrm{def}}$ means it accounts partially for growth behaviour observed according to Fig. 1(a), but only qualitatively. Also, the plastic criterion permits indefinite growth, requiring separate solutions for breakage behaviour where relevant. When implemented and tested, the ratio h_0/h_a is consistently treated as constant [23,25] (and [26–28] too, according to [25]), which raises doubts over how well it accounts for saturation variation. When the elastic solution was subsequently expanded the new equations provided no significant improvements over the original, despite seeming to account for more of the physical parameters [29].

1.1.2. Saturation limiting size

Butensky and Hyman [30] developed a solution based on the physical conditions of where and how liquids fill granule internal volumes, representing the system shown in Fig. 2. They validate it using a method to calculate saturation using a time delayed chemical reaction to stiffen the granules, then calculating the relative quantities of the chemical and the solids for a given size. The equation calculated is:

$$\frac{1}{D_r} = \frac{1}{K_g} - \frac{1}{K_g K_f^{\frac{1}{3}}}\left(\frac{W}{\frac{W_\infty}{K_f}}\right)^{\frac{1}{3}} \tag{4}$$

Where K_g is the dimensionless fraction describing the distance from the outer bounding diameter and the surface of the sphere, nondimensionalised with respect to D_p, and is bounded between 0 and 2 as a physical requisite to ensure that all particles within the granule are wetted, and can be assumed to be around 1 [30].

This can be re-arranged Appendix A to produce:

$$\Delta_{sat} = \frac{K_g D_p}{\left(1-\left(\frac{S}{K_{S_{\max}}}\right)^{\frac{1}{3}}\right)} \tag{5}$$

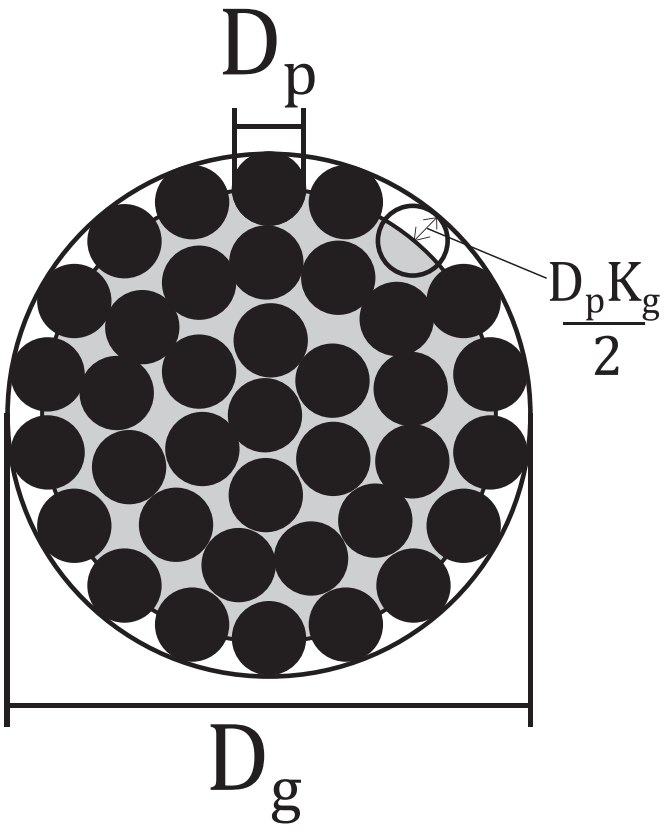

Fig. 2. Simplified diagram showing the physical meaning behind (4). The total saturation (grey) is limited on account of the observed liquid surface layer with the saturation below it being full equal to that of $K_{S_{max}}$. K_g is the dimensionless fraction describing the distance from the outer bounding diameter and the surface of the saturation, nondimensionalised with respect to D_p Recreated based on [30].

This form can easily be compared with the literature, see Fig. 3, where it matches strongly those cases where saturation is tracked [1,5,6,14–16,25]. Note that $K_{S_{max}}$ is the maximum value of saturation before slurry formation, which is a property of the feed and potential air entrapment in the granule centre.

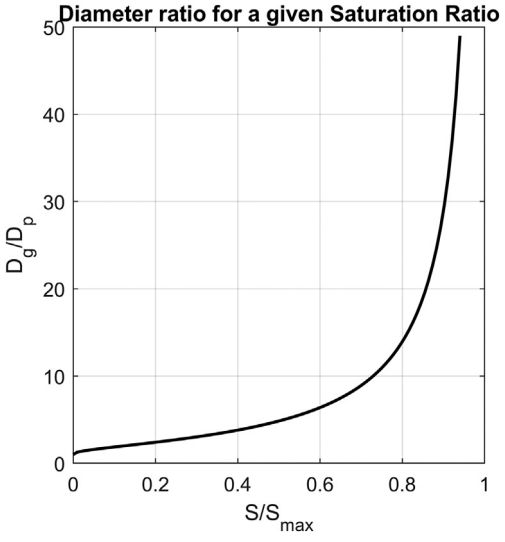

Fig. 3. Eq. (5) plotted, demonstrating the observed rapid increase in growth rate as the granule becomes saturated.

It does not match the liquid to solid ratio relations as strongly because saturation is a function of the Liquid to solid ratio as well as the porosity, which can vary independently. Although it does not account for viscosity, it has been reported that viscosity is not always relevant [15]. The assumed arrangement of the liquid makes sense (Fig. 2), as liquids in a granular material favour forming fewer larger clusters of liquid as this is more stable [31] and such behaviour has been observed when wet granular piles were scanned [32]. As the liquid content increases, the structure merges into larger clusters. Therefore, the liquid in the granules can be assumed to also be formed into such clumps where possible, and in this fashion arrange themselves in a way consistent with Fig. 2. In real granulation, D_p is expressed as a range. In the original experiments, the arithmetic mean of the particle diameters appears to be a suitable value for this [30]. Some experiments with the particle diameters have found that finer particles result in wetter granules. This is likely due to two effects. The first is that since the liquid is found at a distance $D_pK_g/2$ from the surface, smaller particles will lead to a smaller distance from the surface of the liquid. Finer particles will also require a greater degree of saturation for the same total granule diameter compared to larger particles. On the other hand, there are cases when viscosity is relevant, such as for crumbling and high shear granulation. In such cases a dynamic limiting size must be relevant.

1.1.3. Dynamic limiting size

A dynamic limiting size solution was determined by Ouchiyama and Tanaka [33] who calculate the probability that

$$\sigma_{bond} > \sigma_{sep} \tag{6}$$

after granules come into contact. The value of σ_{sep} is derived by consideration of the moments that are applied by contacting forces on the particles from external sources after σ_{bond} has formed. From this, and consideration of the probability of the coalescence over the whole system, Eq. (7) is developed:

$$\Delta_{\text{merge}} = \left(\frac{2^{\alpha-\frac{3\eta}{2}}}{B} Q_M^{\frac{3\zeta}{2}} K^{\frac{3}{2}} \sigma_{\text{bond}}\right)^{\frac{1}{4-\frac{3\eta}{2}}} \tag{7}$$

ζ and η are parameters that adjust the function for plastic or elastic granules. Wet agglomerates appear to behave plastically under unconfined conditions [27], so for plastic granules this gives (8)

$$\Delta_{\text{merge}} = \left(\frac{2^{\alpha}}{B} Q_M^{\frac{3}{2}} K^{\frac{3}{2}} \sigma_{\text{bond}}\right)^{\frac{1}{4}} \tag{8}$$

This is promising as the power matches Watano et al's findings [10] wherein the limiting diameter was found to be proportional to $\left(1/\left(\left(V_i/V_f\right)^2\right)\right)^{(1/4)}$, which is the ratio of the impeller tip speed and the fluidisation velocity for a fluid bed granulator system i.e. related to the strength of separation forces and collision forces. However, the full solution specified by Ouchiyama and Tanaka is a probabilistic one, which makes it less useful as it requires prior knowledge of the kinematic behaviour of the collisions. It also lacks a solid basis for σ_{bond}. Further, it also does not account for saturation which is necessary for determining growth behaviour.

2. Development of a new analytical model

Eqs. (5) and (8) provide two separate cases for the limiting size but they have limitations.

1. They are both lacking one half of the solution, either the dynamic limit for Eq. (5) or the saturation for Eq. (8)

2. Eq. (8) is defined as part of a probabilistic solution, and although the limiting size does not depend on the probability, it limits the model's general applicability.
3. Neither equation describes growth rates which are important in defining the behaviour of a system.

Therefore, the proposed solution sets out to combine the two solutions in a physically meaningful framework.

2.1. Dynamic limit

The model begins with Eq. (6), determining the values of σ_{bond} and σ_{sep} in a deterministic manner.

2.1.1. Bond strength σ_{bond}

A suitable prediction for the bond strength comes from [34]. The authors determine the strength of a bond between two partially saturated cylinders as they are pressed together, shown for sphere surfaces in Fig. 4, before being pulled apart again. The saturation of the cylinders surface is similar to that determined by the limiting case in Eq. (5), as there is the drier boundary with the moisture underneath.

Based on this, from an analogy drawn from cold welding, the following equation is obtained:

$$F_{\text{Bond}} = 0.65\sigma_y \pi r_0 \left(2\varepsilon_{\text{rr}} + \varepsilon_{\text{rr}} + 1 - e^{-K_s\varepsilon_{\text{rr}}}\right) \tag{9}$$

With the analogy being that instead of fresh metal being exposed from beneath an oxide layer as in cold welding, binder rich liquid comes to the surface as the materials are pressed together during agglomeration.

Eq. (9) can be re-arranged to find the bond strength of the final area of contact, which is necessary as spheres coming into contact have an initial contact area of 0. In addition, the value 0.65 is replaced with a constant $K_{\frac{t}{c}}$ which is a constant describing the ratio of the compressive strength to the tensile strength.

$$\sigma_{\text{bond}} = K_{\frac{t}{c}}\sigma_y \left(1 - \frac{e^{-K_s\varepsilon_{\text{rr}}}}{(\varepsilon_{\text{rr}} + 1)^2}\right) \tag{10}$$

Where K_s is a constant related to the immediate strength of the bond without prior compression and is expected to be inversely proportional to viscosity and generally related to saturation in some fashion, especially for saturation values greater than 1 when the surfaces will be wet. In the original paper [34] though K_s is assumed to be 0, and the findings in that original paper seem to tentatively agree with this assessment.

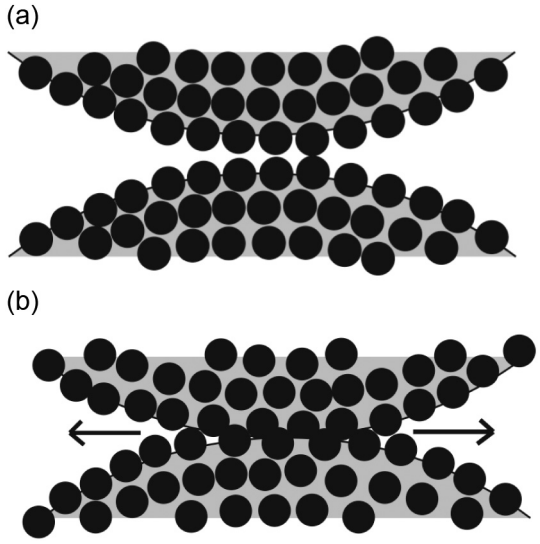

Fig. 4. Diagram of agglomerates wetted to just below the surface before and after contact. (a) Diagram of surfaces of wet agglomerates prior to contact. (b) Diagram of surfaces of wet agglomerates pressing into one another, inducing the capillary bonds and some particles to inter-mingle, initiating bonding.

2.1.2. Radial strain ε_{rr}

To determine the radial strain, the granule is assumed to be isotropic and follow the Poisson's ratio relationship,

$$\varepsilon_{\text{rr}} = -\nu\varepsilon_{zz} \tag{11}$$

from which the following is obtained, noting that E is an observed pseudo-elastic stiffness observed in [35] appropriate for wet agglomerates

$$\varepsilon_{\text{rr}} = -\nu\varepsilon_{zz} = -\frac{\nu\sigma_{zz}}{E} = \frac{\nu Q}{EA} \tag{12}$$

where the negative sign indicates compression. For a plastic sphere [36]:

$$Q = p_0 A \tag{13}$$

So that

$$\varepsilon_{\text{rr}} = \frac{\nu Q}{EA} = \frac{\nu p_0}{E} = \frac{\nu K_H \sigma_y}{E} \tag{14}$$

With K_H being a constant that relates the hardness and the yield strength [36]. The value of Poisson's ratio ν is assumed to be similarly constant. From a physical standpoint, granules do not demonstrate significant elastic behaviour. Therefore, a value of ν below 0.5 would result in a permanent reduction in volume. Such a permanent reduction in volume is considered in the consolidation behaviours. Experimentally, for soils with saturations above 0.6 with significant proportions of fines, the Poisson's ratio tends to be between 0.4-0.5 [37]. As this is the saturation level in most granulation processes where practical growth is applied, the use of a constant Poisson's ratio is taken as a good approximation at this stage.

Note, this implies that the surface radial strain is constant. In plastic deformation experimental testing it was found that the deformed area of a sphere when pressed against a non-deformable surface was found to remain linear with respect to load, supporting the idea of a constant value for radial strain [38]. Another way to consider it comes from [35] which shows that for granular materials, the value E appears to be constant until the agglomerate fractures. This fracture point would then coincide with the appearance of the crumb state for excessive deformations. Considering both at the same time, there is almost no stress per unit strain from 0 strain to 0.4 units of strain, and only a slight raise from 0.4 to 0.5 [39]. Also the bulk behaviour of the granule is relatively stable across a wide range of liquid contents, softening once the liquid solid ratio goes over 100% [39].

2.1.3. σ_{bond} summary

Combining Eqs. (10) and (14) gives:

$$\sigma_{\text{bond}} = K_{\frac{t}{c}}\sigma_y \left(1 - \frac{e^{-K_s\frac{\nu K_H\sigma_y}{E}}}{\left(\frac{\nu K_H\sigma_y}{E} + 1\right)^2}\right) \tag{15}$$

Which may be simplified by recognising that the third term is the nondimensional value relating the amount of strain to the amount of fresh wet area over which to create the bond (which as previously established appears to be relatively constant until crumbing behaviour occurs) and this third term will be referred as the adhesion function.

$$\sigma_{\text{bond}} = K_{\frac{t}{c}}\sigma_y \alpha_{\text{wet}}(\varepsilon_{\text{rr}}) \tag{16}$$

As mentioned, K_s is suggested to be in some way related to the saturation. Therefore, this wet adhesion function is likely tied to (5) in some fashion. This would be consistent with findings showing that critical strain changes with saturation [16], although, as will be explored later, on an individual level the granules can be assumed to have similar internal saturations. One final point regarding this value is that adhesion was not assumed when considering the deformation behaviour of the granules. Adhesion models such as that developed by Johnson, Kendall and Roberts [40], also referred to as the JKR model [41] are designed to balance elastic and adhesive forces against one another within elastic spheres, but here the granules are assumed to be perfectly plastic.

2.1.4. Separation strength σ_{sep}

The expression for σ_{sep} is partly based on the original solution [33]. It defines the separation forces in terms of the maximum moment that will be applied during the process, which comes from the bulk shear motion of the granules. The basic equation for the stress induced by moments around the centre of the bond is:

$$\sigma_{\text{sep}} = \frac{3M}{4\pi^{\frac{3}{2}}A^{\frac{3}{2}}} \tag{17}$$

To calculate σ_{sep} thus requires the moment M and the area of contact A.

2.1.5. Area of contact A

The area of contact can be calculated by considering the normal kinetic energy of the collision of two particles as it dissipates while being plastically absorbed.

$$\int_0^{\delta^*} Q d\delta = E_P = E_{K_N} = \frac{1}{2} V_{C_N}^2 \tilde{m} \tag{18}$$

The relation between compression force and deformation depth for plastic spherical contacts is [36]:

$$Q = p_0 \pi a^2 = p_0 \pi \tilde{R} \delta \tag{19}$$

from which the area can be shown to be proportional to the kinetic energy of the collision, (derivation in Appendix B), in Eq. (20)

$$\pi a^{*2} = A = \pi \sqrt{\frac{4}{3}} \sqrt{\frac{\rho_g}{K_H \sigma_y}} V_{C_N} \sqrt{\tilde{R}\widetilde{R^3}} \tag{20}$$

2.1.6. Separating moment M

In Ouchiyama's work [33], M is further broken down into Eq. (21)

$$M = A_M \frac{g(D,d)}{2^{\alpha}} \tag{21}$$

$(g(D,d)/2^{\alpha})$ is a function of granule diameters related to different cases where volumes can be related to separating forces. A_M is a dimensioned constant of proportionality which relates these forces. A_M is unrelated to the particle sizes beyond the relationship specified through M. $g(D,d)$ is a function which switches between five different cases, however, these can be described satisfactorily with a single function Eq. (22) [33]

$$g(D,d) = \frac{(dD)^{K_\gamma}}{\left(\frac{d+D}{2}\right)^{2K_\gamma - 4}} \tag{22}$$

which provides a sliding parameter K_γ for distinguishing between the original five cases. This in turn can be re-arranged to form Eq. (23):

$$g(D,d) = \left(\frac{\hat{D}}{\bar{D}}\right)^{2K_\gamma} \bar{D}^4 \tag{23}$$

$\hat{D}$ is the geometric mean (GM) and $\bar{D}$ is the arithmetic mean (AM). This arrangement highlights two distinct terms on the right-hand side, the first being the layering component which changes the behaviour depending on the ratio of the two granules colliding, and secondly the "steady" component which is consistent. A second benefit to this arrangement is that, because of AM-GM inequality, the layering component is known to be always <1 while $K_\gamma > 0$.

A_M is less simple, but, since it relates the volume of the granules to the forces, it has known units, see Eq. (24).

$$A_M = \frac{F}{V} = \frac{M}{T^2 L^2} \tag{24}$$

This makes A_M well suited to dimensional analysis, as it has known dimensions, a specific role in the function and is explicitly unrelated to the granule diameter [33].

The summary of this dimensional analysis is as follows. Since A_M is relating the size of the particles to a force, then it is reasonable to assume that it is a function of granule density. In addition, assuming A_M is related to the velocity of the particles (or some other characteristic velocity such as that of an impactor) which is also reasonable, squaring this velocity allows it to correspond to the change in kinetic energy due to such impacts. This leaves another variable, L^{-1}. This can be expressed as Eq. (25)

$$A_M \propto \frac{M}{L^3} * \left(\frac{L}{T}\right)^2 * \frac{1}{L} \tag{25}$$

Applying a nondimensional constant then gives Eq. (26)

$$A_M\left(\rho_g, {V_{\text{ch}}}^2, L_{\text{ch}}\right) = \frac{K_A \rho_g {V_{\text{ch}}}^2}{L_{\text{ch}}} \tag{26}$$

Where L_{ch} is a characteristic length scale. It cannot be the granule diameter, and it must be some variable that results in lesser intensity of separation forces as it grows and can be described independently of the granulator system. A suitable analogy then is the "mean free path", λ, as applied in kinetic theory of gasses. Due to inelastic collisions intrinsic to granular materials [42], and the fact that the maximum separating moment of the collisions is oblique, and that the collisions must be significant given that minor collisions will enhance the bond, this is more complex than the simpler molecular case. The resulting λ_{ch} is likely related to the turbulence of the granular flow, as this will result in more tangential contacts and more rotation of the coalescing granule pair.

Combining and rearranging Eqs. (21), (23), and (26) gives (27)

$$M = \frac{A_M\left(\rho_g, {V_{\text{ch}}}^2, \lambda_{\text{ch}}\right)}{2^{\alpha}} \left(\frac{\hat{D}}{\bar{D}}\right)^{2K_\gamma} \bar{D}^4 = \frac{K_\alpha \rho_g {V_{\text{ch}}}^2}{\lambda_{\text{ch}}} \left(\frac{\hat{D}}{\bar{D}}\right)^{2K_\gamma} \bar{D}^4 \tag{27}$$

Since α is just a constant tied to the collision behaviour, (2^{α}) is incorporated into K_A to form K_α, the agitation constant.

2.1.7. σ_{sep} summary

Collecting Eqs. (17), (20), and (27) gives

$$\sigma_{\text{sep}} = \frac{3M}{4\pi^{\frac{3}{2}}A^{\frac{3}{2}}} = \frac{3\frac{K_\alpha \rho_g {V_{\text{ch}}}^2}{\lambda_{\text{ch}}} \left(\frac{\hat{D}}{\bar{D}}\right)^{2K_\gamma} \bar{D}^4}{4\pi^{\frac{3}{2}}\left(\pi\sqrt{\frac{4}{3}}\sqrt{\frac{\rho_g}{K_H\sigma_y}} V_{C_N}\sqrt{\tilde{R}\widetilde{R^3}}\right)^{\frac{3}{2}}} \tag{28}$$

2.2. Dynamic limit defined

Substituting Eqs. (28) and (16) into (6) gives

$$K_{\frac{t}{c}}\sigma_y\alpha_{\text{wet}}(\varepsilon_{\text{rr}}) > \frac{3\frac{K_\alpha\rho_g {V_{\text{ch}}}^2}{\lambda_{\text{ch}}}\left(\frac{\hat{D}}{\bar{D}}\right)^{2K_\gamma}\bar{D}^4}{4\pi^{\frac{3}{2}}\left(\pi\sqrt{\frac{4}{3}}\sqrt{\frac{\rho_g}{K_H\sigma_y}}V_{C_N}\sqrt{\widetilde{R\bar{R}^3}}\right)^{\frac{3}{2}}} \tag{29}$$

This can be rearranged (see Appendix C) to form

$$\left(\frac{\hat{D}}{\bar{D}}\right)^{2K_\gamma-4}\frac{\left(\bar{D}\bar{D^3}\right)^{\frac{3}{4}}}{\hat{D}^2} < C_m\ \frac{K_{\frac{t}{c}}}{K_\alpha K_H^{\frac{3}{4}}}\alpha_{\text{wet}}(\varepsilon_{\text{rr}})\frac{{\sigma_y}^{\frac{1}{4}}}{{\rho_g}^{\frac{1}{4}}}\frac{{V_{C_N}}^{\frac{3}{2}}}{{V_{\text{ch}}}^2}\lambda_{\text{ch}} \tag{30}$$

And in turn, by defining $d = r_d D$ and noting that the merged granule diameter between two granules D and $r_d D$ is $D\sqrt[3]{1+r_d}$ (full derivation in Appendix D) gives

$$\Delta_{\text{bond}} < C_m\frac{K_{\frac{t}{c}}}{K_\alpha K_H^{\frac{3}{4}}}\alpha_{\text{wet}}\frac{{\sigma_y}^{\frac{1}{4}}}{{\rho_g}^{\frac{1}{4}}}\frac{{V_{C_N}}^{\frac{3}{2}}}{{V_{\text{ch}}}^2}\lambda_{\text{ch}}\frac{(1+r_d)^{2K_\gamma-2\frac{11}{12}}}{{r_d}^{K_\gamma-3}(1+{r_d}^3)^{\frac{3}{4}}} \tag{31}$$

Δ_{bond} is now the limiting size that the merged granule can reach. The presence of $1/r_d^{K_\gamma-3}$ means that while $K_\gamma > 3$, as $r_d \to 0$, $\Delta_{bond} = \infty$, and the bond does not limit the ability for such mergers to occur. This is relevant, not just for layering systems but also for heterogeneous systems, since some of the granules would grow faster than the bulk by consolidating with smaller feed granules, even if this means they grow larger than the system Δ_{bond}.

The granule size ratio term also has the interesting property that, for values of $K_\gamma > 4$, below r value of around 0.2 it favours dissimilar granules and above around 0.2 it favours the merging of larger granules. This would explain the contradictory results observed in [43] where the overall behaviour of the granule growth is best described with an equipartition of kinetic energy kernel which favours large-small coalescence, but the tracer distribution appeared to be better described by a shear kernel which favoured large-large coalescence.

Eq. (31) can be further simplified by assuming that $V_{C_N} \propto V_{\text{ch}}$, which makes sense for granulation systems where the sources of input kinetic energy will increase both in proportion. Doing so allows (30) to be written in the form

$$\Delta_{\text{bond}} < C_m\frac{\lambda_{\text{ch}}}{K_\alpha \text{St}_{\text{def}}^{\frac{1}{4}}}K_H^{\frac{3}{4}}K_{\frac{t}{c}}\alpha_{\text{wet}}\frac{(1+r_d)^{2K_\gamma-2\frac{11}{12}}}{{r_d}^{K_\gamma-3}(1+{r_d}^3)^{\frac{3}{4}}} \tag{32}$$

There are three major terms, the agitation term, the adhesion term, and the size variation term. The presence of $\text{St}_{\text{def}}{}^{-\frac{1}{4}}$ is promising, as it retains the relationship reported by Tardos et al [44] describing Watano et al's work [10], where the average granule size was related to $({V_i}^2)^{-\frac{1}{4}}$, and St_{def} is directly proportional to V_c^2.

2.3. Yield strength σ_y

Since the yield strength is a factor in St_{def}, a brief consideration is relevant. There has been much work on this topic, relating yield strength to porosity, interparticle friction and viscosity, as well as other factors. For this work, (33) is used, which accounts for many of these factors [45], which combines a capillary [46] and a viscous [47] strength equation linearly, along with a factor to account for the aspect ratio's contribution to the strength.

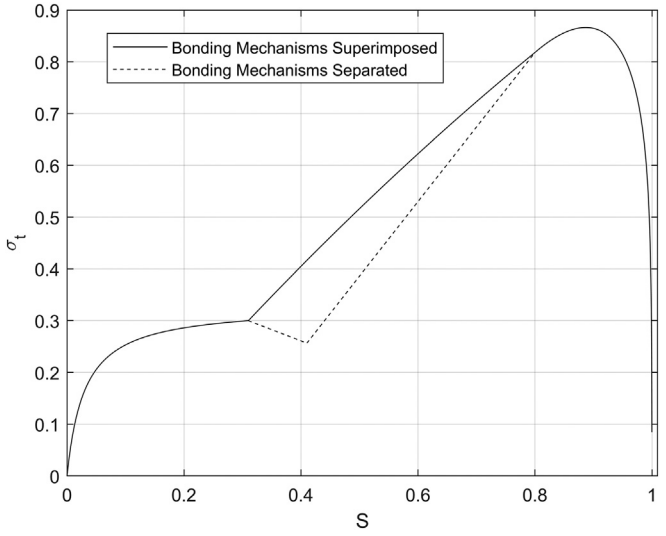

Fig. 5. strength of agglomerate as saturation varies, reproduced based on previous data [48,49]. The strength plateaus initially from pendular bonds forming, and then a linear growth occurs as capillary bonding connects multiple particles with the same droplet, and eventually the strength drops sharply as the gas interface no longer exists to provide surface tension within.

$$\sigma_y = \text{AR}^{-4.3}S\frac{1-\varepsilon}{\varepsilon}\left[6\frac{\gamma\cos\theta}{D_{p_{3,2}}}+\frac{81}{128}\frac{1-\varepsilon}{\varepsilon}\frac{\pi\mu V_c}{D_{p_{3,2}}}\right] \tag{33}$$

Although Eq. (33) is linear with respect to saturation, note that saturation and yield strength have a complex relationship [48,49].

Notice that from $S = 0.8$ onwards in Fig. 5 there is only one line, and $K_{S_{\max}}$ appears to typically be larger than 0.8 [30]. Also, in this region the strength is relatively indifferent to the saturation until $S > 1$. Based on this an assumption is made that below the surface boundary, the saturation is equal to $K_{S_{\max}}$, and this bulk saturation is what provides the strength of the granules, so long as $S < K_{S_{\max}}$, after which the solution is assumed to result in a slurry. Relatively constant behaviour over a wide range of added liquid has been reported [39], supporting this assumption. Also, for a wide range of liquid to solid system ratios, the granules themselves have relatively constant saturations [50], again suggesting this assumption is reasonable.

Interestingly, the idea that the yield strength is related to the velocity suggests that $St_{def} \propto V$ for high Ca values, and $St_{def} \propto V^2$ for low Ca values. Such a relationship, or rather the implication of such a relationship, has also been reported [22].

2.4. Consolidation

To account for growth rates, the dominant time dependent effect is assumed to be consolidation. This is because consolidation affects both the yield strength and the saturation simultaneously. A suitable model to describe consolidation is given in Iveson et al [51]. They show that the observed porosity can be described by Eq. (34).

$$\frac{\varepsilon-\varepsilon_{\min}}{\varepsilon_0-\varepsilon_{\min}} = e^{-k_\varepsilon N} \tag{34}$$

with k_ε being a coalescence parameter and N being the number of revolutions which simply a nondimensionalised measure of time. This form is consistent with measured changes in porosity in a high shear mixer as well [7], which is promising as it suggests the consolidation behaviour is consistent between devices, further demonstrating the universality of these solutions.

The value of k_ε changes with several variables, among which is the apparent inverse proportionality to the yield strength [51,52] and the

kinetic energy of the collisions [53]. The finding that the granules are inversely proportional to ($\mu^{0.26}$) could be a result of the yield strength only partially being related to the viscosity with changing velocity [52], as described above in Section. 2.3. Based on these observations and considering possible relations the value of k_ε that best matched observed behaviours was found to be:

$$k_\varepsilon = k_{\varepsilon_A} e^{\frac{1}{-k_{\varepsilon_B} St_{def}}} \tag{35}$$

Where k_{ε_A} and k_{ε_B} allow appropriate scaling to be applied depending on the rate of collisions and the energy of those collisions respectively. By combining and rearranging Eq. (34) and Eq. (35) the following can be found:

$$\varepsilon = \varepsilon_{\min} + (\varepsilon_0 - \varepsilon_{\min}) e^{-k_{\varepsilon_A} e^{\frac{1}{-k_{\varepsilon_B} St_{def}}} t} \tag{36}$$

Because St_{def} itself depends on the porosity this needs to be calculated numerically, although a final expected size can be found by setting ε_{min} to an assumed final porosity appropriate to the system. This equation has a similar form to the Arrhenius equation [54], particularly considering that St_{def} measures the ratio of the granule deformability to the kinetic energy of the average granules, which matches the activation energy and temperature relation of the Arrhenius equation.

As Eq. (36) is an exponential decay function, the initial porosity affects the initial rate of growth while the final porosity affects the final size. Similar arguments could be made for ε_{min} itself, considering how intragranular porosity increases as St_{def} increases [55]. This is also consistent with theoretical work [56] demonstrating how ε_{min} can increase for higher acceleration forces, and a reported linear relationship between the ratios of the force applied to the force providing the minimum porosity, and the porosity value and the minimum porosity determined [57]. This is also consistent with the finding that the "elongation" is proportional to the St_{def}, [58] and this elongation would dilate the granules.

However, since the exact manner in which these terms are related is still not clearly understood, the value of ε_{min} will be assumed to be constant. The liquid to solid ratio will also be treated as constant despite the evidence mentioned previously concerning evidence showing that for certain cases it may decrease during consolidation due to evaporation or even increase due to dehydration reactions of the granulation materials [20,23,59].

2.5. Summary of new model

The new model, which depends on all the above features, is summarised as the "Adhesion-Cohesion" model. This highlights the two part nature, where the granules are *able* to grow if they have sufficient moisture such that they remain cohered together via Eq. (5), and they *can* adhere if, on contact, they satisfy Eq. (31). The diameter of the granule is limited to the smaller of the two limits. As the Cohesion component is highly dependent on the saturation, the consolidation is sufficient to describe the change in size. By reducing the total pore space for a given liquid volume, the saturation increases, which increases the value of Δ_{sat}. The assorted material and system dimensionless constants, all defined using K along with a subscript, are defined clearly, so that they can be adjusted appropriately depending on the material and systems as the model is further developed. Some preliminary values are available for them, based on previous research, however these should not be assumed to be universal but rather simply a starting point. These are a result of either the mechanical requirements of the model, such as those specified for K_g, or from experiments using specific particle-binder combinations, such as the value used for $K_{\frac{t}{c}}$ previously mentioned. K_α is a dimensionless constant which accounts for externalities not considered elsewhere in the separation behaviour, and being derived fresh, will need investigation to determine the range of values applicable in different granulation systems.

3. Results

The following graphs are the size predictions based on the conditions of a limiting size assuming only equal size granules ($r_d = 1$) are merging. Eqs. (31) and (5) are used together, with the limiting size taken to be the smaller of the two. Whether or not the granules turn into a slurry is simply determined by whether the granule saturation is larger than $K_{S_{max}}$, in accordance with the growth behaviour demonstrated in Fig. 1. It may be possible for granules in certain systems to not form into a slurry with an excess of saturation, such as in very high viscosity systems, but in such cases a different form of the yield strength equation may be necessary as well and so can't be assumed to be within the scope of this solution.

Eqs. (5), (31) and (36), combined can be used to demonstrate the same distribution of dominant mechanisms in the classical mechanism map format. The plots are given using the simplified case of a constant minimum porosity for the reasons mentioned in Eq. 2.4 though the value of ε_{min}, and other variables, listed in Table 1 are based on relatively common or accepted values drawn from the literature. Other values, such as K_α are then defined at the values shown to demonstrate the growth regimes that can be observed and would vary according to each system according to any number of reasons (see [60], where only changing the number of blades in a high shear granulator nonetheless results in significantly different behaviour). K_γ is set based on the case described by 4.5 in [33], and this also lines up with the behaviour described in [43] for reasons previously mentioned.

3.1. Final size prediction

Fig. 6 simply describes the relative granule size at the minimum porosity, which is treated as the same across the map.

The regions described as "crumb" and "nucleation only" from Fig. 1 can be seen in Fig. 6, as well as the region where growth does occur, which would be the steady and induction growth regions on that map. The letter-number pairs relate to various growth phenomena described in Eq. 3.3.

3.2. Growth behaviour prediction

The consolidation Equations, Eq. (36), can be applied to calculate the change in porosity over time, and for each V_l/V_s, a unique saturation can

Table 1
The variables used in the results when not specified otherwise.

Variable	Value
$K_{\frac{t}{c}}$	0.65
K_α	253
K_H	2.8
λ_{ch}	10 mm
$\alpha_{wet}(\varepsilon_{rr})$	1
D_p	50 μm
K_g	1
$K_{S_{max}}$	1
r_d	1
K_γ	4.5
μ	1 mPas
γ	0.072 N/m
θ	30
AR	1
ε_{min}	0.3

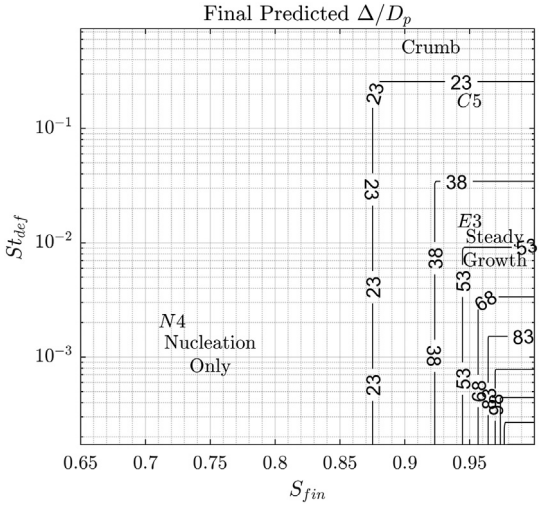

Fig. 6. Limiting size predicted for different conditions. (S_{fin}) used to describe the final saturation reached, to differentiate between the final saturation and the maximum saturation the system can have before turning into a slurry. The values along the contours specify the final predicted dimensionless size (Δ/D_p) of the granules under the conditions specified.

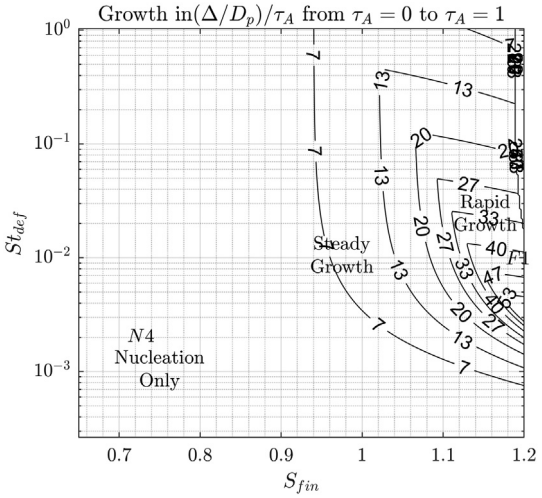

Fig. 7. The growth rate between $\tau_A = 0$ and $\tau_A = 1$. The numbers along the contour lines indicate the increase in relative granule size per τ_A over this time span within the boundary.

be found. Therefore, the growth behaviour can be predicted. Using the values in Table 2, Figs. 7, 8 and 9 show the growth behaviour at sequential points in time, representative of early, middle and late stages of growth.

The term τ_A is used to refer to the dimensionless time as defined by $\tau_A = tk_{\varepsilon_A}$. The use of scaling according to time has been shown to work in the past [61].

In Fig. 7, note the presence of the rapid growth, the steady growth and the nucleation regions, and that the growth rate diminishes as the granule deformation approaches the crumb region but is still faster than the low deformation region where consolidation isn't sufficient to develop the levels of saturation required to grow beyond nuclei.

In Fig. 8 much of the region previously described as rapid growth has turned into slurry, or some has ceased growing, being in the crumb regime, while the steady growth region continues to grow. Also note the progress of the growth moving downwards to the low deformation number region.

And finally, in Fig. 9 the steady growth region has slowed down in growth rate, as it approaches equilibrium. The region around $St_{def} = 10^{-3}$ has started growing at significant rates, though due to the changing rate nature of induction, it is easier to observe on individual plots at points in the region over time.

3.3. Specific growth patterns predicted

The growth predictions for specific points on the map are shown in the following results. In each case, the combination of the various agitation variables defined by Eq. (37) is noted.

Table 2
Constants related to the consolidation process.

Variable	Value
ε_0	0.5
ε_{min}	0.3
k_{ε_A}	1e-3 1/s
k_{ε_B}	1e3

$$\Omega_{\text{def}} = \frac{K_\alpha \text{St}_{\text{def}}{}^{1/4}}{\lambda_{\text{ch}}} \tag{37}$$

Ω_{def} is useful in that it would be hard to measure the precise value of K_α and St_{def} in any real system, so instead this constant describes the combined effect of the intensity and frequency of the collisions the granules experience, to highlight how different feedstocks might react differently even within the same granulator which can nonetheless be described using the equations above. The choice for the plots is based on previous descriptions of the various accepted granule growth behaviours [8], as well as the various growth behaviours Previously described in the introduction. Fig. 10 shows the plots of the growth patterns with parameters specified by Table 3 displayed over dimensionless time.

Fast growth without limit observed in systems such as drum granulation with coarse particles with low viscosity binders in drums, or medium viscosity binders in mixers [18,39,52,62]. The larger D_p in this case accounts for this, while the low Ω_{def} would be more expected in drum granulation cases.

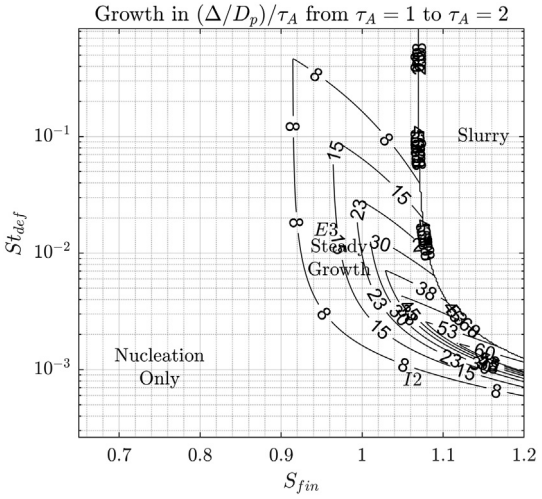

Fig. 8. The growth rate between $\tau_A = 1$ and $\tau_A = 2$. The numbers along the contour lines indicate the increase in relative granule size per τ_A over this time span within the boundary.

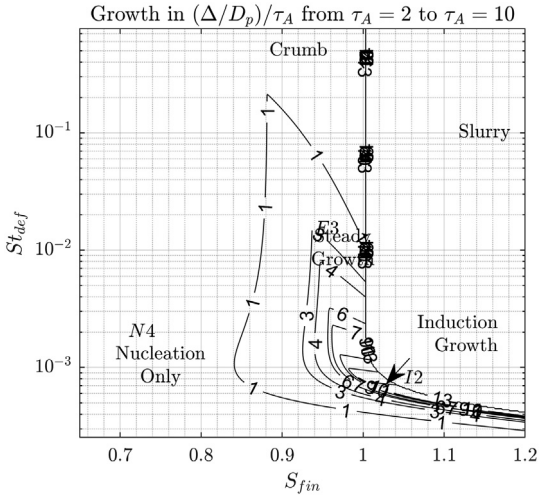

Fig. 9. The growth rate between $\tau_A = 2$ and $\tau_A = 10$. The numbers along the contour lines indicate the increase in relative granule size per τ_A over this time span within the boundary.

Induction behaviour can also be shown using this solution. Once induction is initiated, the growth rate is rapid enough to cause indefinite growth, though the granulation is usually stopped once the growth hits this state [26,39]. The low Ω_{def} and the low particle sizes contribute to the induction behaviour, though lower values of k_{ε_B} would provide similar results and are likely related.

The equilibrium growth, which is found when the saturation is below the amount required for a slurry. In the case shown in Fig. 10, the size is at a boundary where changes in both the saturation and the deformation number can result in changes in the granule size. This is the ideal growth regime to be in as it is controllable, and found in [4,9,11,16,18,21,23,39].

Nucleation is the result of insufficient binder to grow the granules. Because the distribution isn't perfectly even in granulation processes, the droplets that are initiated result in localised higher saturation, which result in the observed nuclei and the size dependence on the droplets, in accordance to nuclei size growth observed by [63] and [64]. The generally observed nuclei limited growth is found in [15,16,

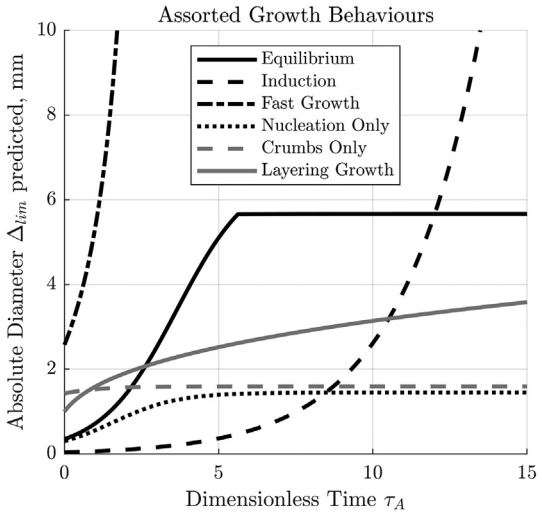

Fig. 10. Growth predictions for various circumstances, cases specified in Table 3. Equilibrium growth is E3 in Figs. 8 and 9. Induction (with no limit) is I2 in Figs. 8 and 9. Fast growth (with no limit) is F1 in Fig. 7. Nucleation is N4 in Figs. 7 and 9. Crumbs only is C5 in Fig. 9. Layering growth applies a different algorithm based on Eq. (32) to test the effect of variations in granule diameters and is shown for comparison.

Table 3
Growth cases determined by the Adhesion-Cohesion with $r_d = 1$.

Growth case	Code	Ω_{def}	S_{fin}	D_p
Equilibrium	E3	4500	0.978	50 μm
Induction	I2	2250	1	5μ m
Fast Growth	F1	2250	1.2	500μm
Nucleation Only	N4	4500	0.9	50 m
Crumbs Only	C5	16000	0.99	500μ m

27,65] for low saturation and no observed growth, and the same can be said for all of the previously mentioned saturation cases previously mentioned in Section 1.1.2.

The Crumb region is in fact not a clearly defined region, other than granule diminution due to excessive agitation. This is further muddied by the fact that for some granulation conditions, the "crumb" state is temporary [66], before the mixture actually forms into a slurry. [67] test the breakage of nucleated, rather than pressed, pellets, which would be more realistic comparison for reasons mentioned previously, though [45] does show that the number of survivors, and hence, Δ_{bond} stabilises quickly into the more stable smaller size. Crumbling can also be the result of insufficient saturation but if the granules are introduced at a larger size due to being manufactured in that shape the binder will re-distribute into the lower size. Other experiments finding the stability of low size of crumbs are [18,58]. If ε_{min} is allowed to increase for high deformation numbers, then this effect is even more drastic, but can also lead to the case where an oversaturated slurry results in granules, though this has been observed in [12] so may be plausible. Viscosity is noted to be relevant in the development of granules beyond crumbs, and this may be explained through the increase in yield strength due to the viscosity, particularly in high velocity granulation systems, but other possibilities are considered in the discussion.

Layering can also be predicted, and it matches the general trends found in [12,68]. The prediction comes from the r_d terms, and the growth rate depends on the rate of interaction, which would be linked to λ_{ch}. It would also be limited by the saturation, though layering systems often include binder with the feed particles. [11] interestingly demonstrates the effect of providing enough saturation to nucleate the granules evenly. In such a case the layering decreases, as there are fewer free feed granules that are not nucleated, and the r_d term is relatively linear above $r_d = 0.2$, which would also suggest a limit on the size of layering growth if a finite feed is provided, which is observed in [12].

The layering behaviour is quite important as it accounts for the effect of the variable r_d, in turn which would provide the slow growth period after the main growth has finished as observed in other studies [9,23]

4. Discussion

The model presented here is derived from three basic principles.

1. Regardless of the original distribution, moisture will move to a stable configuration in the centre of the granule according to capillary pressure
2. Growth occurs if the diameter is smaller than that which the current saturation capacity allows as defined by Eq. (5)
3. Growth is inhibited if the bond strength is too low to survive the forces applied during processing.

Using this model with a range of input parameters, a variety of phenomena in granulation can be defined. The model matches observations of 'nucleation only' and crumb behaviour. When consolidation is considered, the model is also capable of predicting the trends in growth rate behaviour during wet agglomeration. Slurry behaviour is simply defined by the occurrence of a global saturation greater than a prescribed value, assumed here as 1, so that slurry formation is predictable too.

The model is still limited in some respects. A better model for consolidation rate would allow higher quality predictions of growth rate. Additionally, there are different available methods to calculate yield strength although they ascribe similar importance to capillary, frictional and viscous strength effects, as noted in Section 2.3. Finally, certain values are assumed to remain constant such as λ_{ch} and α_{wet}. The former is assumed to be a function of the system, while the latter is a function of the saturation limit. This is an unresolved issue and is a topic for further work, noting that the surface saturation will be very hard to track, especially since the surface saturation will also be lower than the average saturation of the bulk of the granule, not just due to capillary inward pressure but also due to evaporation from the surface. As noted in Eq. (31), the variation in granule size is a factor in the bond limiting size. If there is a wide range of granules, then this would result in higher average granule sizes and generally affect the growth patterns observed in a way that would change over the course of the granulation. This would need to be accounted for and would be affected by the particular details of the granulator. Nonetheless, the results presented here are consistent with many previously established findings. The Adhesion-Cohesion model still requires a large number of parameters to develop a prediction, but overall it should allow a better understanding of the internal behaviours affecting the granulation process. Further, many of these parameters are able to be studied outside the complexities of granulation.

One finding that was surprising, though reasonable in hindsight, was that the model suggests the final granule size is inversely proportional to V_c while the growth rate is directly proportional to V_c. This, in part, would explain why finding a single solution to determine final granule size has been such a challenge. The implication is that, until the final consolidation is reached, the granule size is proportional to V_c. For granulation systems relying on self-selection to remove granules at (or above) a desired size such as disc pelletisers, the interactions of the properties will be much harder to analyse because heterogeneity may still be present internally. For example, if a granule has high porosity, but also high liquid content, then it would have the same saturation as a well consolidated granule with lower porosity and lower liquid content, but they would have different strength values for the same size.

Since the minimum porosity expected is not always reached (nor is it the same as an external measurement of porosity such as wet tapped porosity) then the "true" value of $K_{S_{\max}}$ might be greater than the measured $K_{S_{\max}}$. This would explain how some published data contains results that match Eq. (5) for an $K_{S_{\max}}>1$ [14]. The size limit described by Eq. (5) is better considered in terms of the overall "Cohesion criterion" it represents rather than as a "Saturation limit", since there are other effects which might alter this behaviour. For example, bentonite has demonstrated an ability to increase the size of pellets for a given liquid addition. The simplified form of the Adhesion criterion Eq. (32) is strongly supported by experiments with a fluidized bed granulator [10], which given that it is implicitly based on the cohesion criterion, suggests that the same fundamental behaviours described in the combined model are relevant in such systems.

This porosity change dependence may also explain other behaviours. If the feed porosity is not precisely controlled, which is unlikely to be practical in many applications, then it can result in different growth behaviours for the same mixture. The same mixture that in one batch grows with induction behaviour due to high initial porosity may begin the process again with lower porosity and grow much faster, which is found in [27] for the small particle size, high viscosity case.

In general, Eq. (5) suggests, for a low intensity system where the saturation is the limiting parameter and granulation is desired to convert from small feed particles to large granules, that saturation control is crucial. The predicted difference in granule size between 1% saturation at low saturation values and 1% at high saturation values is very large. This sensitivity is most easily observable when granulating very small feed into very large granules.

Because when the granules contact, they must also satisfy the adhesion criterion, i.e. the dynamic size limit, then the effect mentioned above is balanced somewhat. Because the size ratio term promotes growth between larger and smaller granules, this means that larger, and therefore more highly saturated granules have a wider range of collision parameters which can allow them to merge with smaller, less saturated granules. Upon merging, the combined granule has a reduced saturation, which results in less oversize granules than would be predicted if only the saturation was controlling the growth. The kinetics also slows the rate of growth to some extent by the need for appropriate collisions, and this in turn allows the saturation to get as close to $K_{S_{\max}}$ as it does, especially when the real implications of the moisture being lost to evaporation over time is considered in practise.

That the fastest growth occurs initially in the high St_{def}, high S_{fin} corner of the map, and slows down in rate for lower S_{fin} and is delayed in time for lower St_{def} matches the qualitative behaviour described in Fig. 1, and indeed the various findings listed in [8]. The fashion in which the growth map changes over time is also of note and offers a method to obtain consistent product from granules using uncertain feedstock. Often, granule size is controlled merely by stopping the process when the appropriate size has formed [2]. However, for batch processes where the granules are limited by the separation forces, a more precise method would be to perform higher speed granulation and then slowly reduce the velocity until the desired granule size is reached.

As Pohl and Kleinebudde [3] pointed out in 2020, although the utilisation of saturation and deformation behaviour is logical and has been successful, there has been almost no noticeable recent progress, especially with regards to introducing other dimensionless parameters. This paper aims to begin such progress using three dimensionless parameters, with explicit reasoning behind them, and some dimensioned parameters which are tied to system variables.

A final note on the findings of this model. The bond strength model was derived from purely mechanical interactions, yet the Arrhenius type equation used for consolidation and the mean free path parameter both appear to provide links to kinetic chemistry. A potential direction of research would be to consider "Granular temperatures" [69]. Given that granulation is essentially physically interacting the granules and determining which bonds result in growth this would allow further analogies to be drawn between these two processes.

5. Conclusion

By considering the granule size purely in terms of the limiting size (determined by saturation and also bond strength versus separation forces), an analytical model for granulation has been developed which is consistent with previous literature. This model was expanded to develop a growth model to account for consolidation. From this a gradual transition between rapid, steady, and induction-based growth behaviours was obtained consistent with classical growth regime maps. Various non-dimensional constants, as well as the mean free path, have been introduced allowing the model to be adjusted for a wide range of granulator conditions. These constants, and how they relate to the process could provide the basis for further research. There are some limitations to the current model. Some are due to the nature of granulation itself, being intrinsically time-dependent and stochastic in nature, which is hard to capture in a simple analytical model. Others are due to a lack of quantified studies into the process of consolidation and other granular physical properties such as yield strengths and bond strengths. Despite these limitations the proposed model appears to be a promising topic for further investigation, and it is currently being implemented into a DEM model to simulate and control granule size distributions in a drum granulator. This ongoing work will also allow direct observation of how kinematic behaviour affects the granulation process.

Nomenclature

A	Area
a	radius of contact area
A_M	Constant of proportionality relating the granule volume to the force applied
AR	aspect ratio of constituent particles
B	Separating force coefficient
C_m	Constant related to merging particles
Ca	Capillary number, defined by $\frac{d_p \dot{\varepsilon} \mu}{\gamma \cos\theta}$
D	Granule diameter
Means	
$\tilde{D}$	Harmonic Mean
$\hat{D}$	Geometric Mean
$\bar{D}_r$	Arithmetic Mean
D_p	feed particle diameter
$D_{p_{3,2}}$	surface mean diameter of the particles
E	material stiffness, Young's modulus for elastic materials
E_P	plastic deformation energy
E_{K_N}	kinetic energy
e_{rest}	Coefficient of elasticity
F_{Bond}	force required to break the bond
K_f	interparticle spacing occupied by void/gas volume
K_g	liquid free surface proportional to the feed diameter
$g(D,d)$	Function which relates the granule diameter to the lever of the maximum moment
h_0	height of liquid surface layer
h_a	asperity height
K	constant relating to contact stiffness
K_s	constant relating the strain to bonding area
$K_{\frac{t}{c}}$	constant relating the tensile to the compressive strength
K_H	Constant relating hardness to the yield strength
K_A	constant relating the characteristic velocity, mean free path and granule density to the separation stresses
K_α	K_A with α included from same function. "Agitation Constant"
k_{ε_A}	constant connecting how the rate of collisions affects the consolidation behaviour
k_{ε_B}	constant connecting how St_{def} of impacts affects the consolidation
L_{ch}	Characteristic length derived from dimensional analysis ofA_M
K_γ	constant relating the granule diameter to various force cases
M	Moment
m	mass
p_0	pressure applied by spherical contact
Q	compressive force
$\bar{D}_r$	granule diameter to feed particle ratio
r_0	initial contact radius
r_d	relative size of the smaller to the larger granule
R	Radius of granule
St_{def}	Stokes deformation number, $\frac{V_c{}^2 \rho_g}{\sigma_y}$
St_v	Stokes viscous number, $\frac{4\rho_g V_c \bar{D}}{9\mu}$
S	saturation
$K_{S_{\max}}$	maximum granule saturation before slurry formation
S_{fin}	the final saturation reached for a given ε_{min} and V_l/V_s
t	time
V_i	impeller tip speed
V_f	velocity of fluidising air flow
V_l	Volume of liquid
V_s	volume of solids
V_p	pore volume
$V_{l_{\max}}$	Maximum volume of liquids that can fill a granule, defined in terms of a ratio
V_{ch}	characteristic velocity
V_c	Collision Velocity
V_{C_N}	normal Collision Velocity
W	Weight of granulating liquid per unit weight of solid
W_∞	Weight of granulating liquid per unit weight of solid when $\bar{D}_r \to \infty$
α	constant related to separating moment type
$\alpha_{\mathrm{wet}}(\varepsilon_{\mathrm{rr}})$	function of area of contact and intermingling of granules
γ	surface tension
Δ	Diameter limit for granules for given conditions
Δ_{sat}	Diameter limit restricting growth based on saturation
Δ_{merge}	the minimum diameter of granules that can merge for $d = D = \Delta_{merge}$, equal to $\frac{\Delta}{\sqrt[3]{2}}$
δ	deformation
ε_{rr}	radial strain
ε_{zz}	axial strain
ε	porosity
ε_{min}	minimum porosity
ε_0	Porosity at the start of consolidation
ζ	constant related to plasticity, 1 for plastic, 2/3 for elastic
η	constant related to plasticity, 0 for plastic 2/3 for elastic
θ	contact angle
λ_{ch}	mean free path between granules
μ	viscosity
ν	Poisson's ratio
ρ_g	granule density
σ_y	yield strength
σ_{bond}	bond strength
σ_{sep}	separation stress
σ_{zz}	axial stress
τ_A	Dimensionless time for scaling purposes, $\tau_A = \mathrm{t} \times k_{\varepsilon_A}$
Ω_{def}	Combination of all agitation variables

Declaration of Competing Interest

The authors declare that they have no known competing financial interests or personal relationships that could have appeared to influence the work reported in this paper.

Acknowledgements

The authors would like to acknowledge the M2A funding from the European Social Fund via the Welsh Government (c80816) and TATA Steel that has made this research possible and helped provide grounding for the practical limitations inherent to industry which helped drive the development of the model.

Appendix A. Saturation re-arrangement

The original equation from [30]

$$\frac{1}{\bar{D}_r} = \frac{1}{K_g} - \frac{1}{K_g K_f{}^{\frac{1}{3}}} \left(\frac{W}{\frac{W_\infty}{K_f}} \right)^{\frac{1}{3}} \tag{A.1}$$

$$\frac{1}{\bar{D}_r} = \frac{1}{K_g} \left(1 - \frac{1}{K_f{}^{\frac{1}{3}}} \left(\frac{W}{\frac{W_\infty}{K_f}} \right)^{\frac{1}{3}} \right) \tag{A.2}$$

$$\bar{D}_r = \frac{K_g}{\left(1 - \left(\frac{W}{W_\infty} \right)^{\frac{1}{3}} \right)} \tag{A.3}$$

f describes the amount of internal volume which is occupied by voidage within a given granule, and its meaning is captured within the subsequent $K_{S_{max}}$, which also accounts for this.

$$W = \frac{m_l}{m_s} = \frac{\rho_l V_l}{\rho_s V_s}, \quad W_\infty = \frac{\rho_l V_{l_\infty}}{\rho_s V_s} = \frac{\rho_l V_{l_{max}}}{\rho_s V_s} \tag{A.4}$$

$\bar{D_r}$ = final granule size to particle size ratio

$$\bar{D_r} = \frac{\Delta_{sat}}{D_p} \tag{A.5}$$

$$\frac{\Delta_{sat}}{D_p} = \frac{K_g}{1 - \left(\frac{\frac{\rho_l V_l}{\rho_s V_s}}{\frac{\rho_l V_{l_{max}}}{\rho_s V_s}}\right)^{\frac{1}{3}}} \tag{A.6}$$

S is the liquid saturation of the pores, which can be defined as

$$S = \frac{V_l}{V_p} \text{ as by definition } V_l = V_p S \tag{A.7}$$

$$\frac{\Delta_{sat}}{D_p} = \frac{K_g}{1 - \left(\frac{\rho_l}{\rho_g}\right)^{\frac{1}{3}} \left(\frac{\frac{V_p S}{V_s}}{\frac{V_p K_{S_{max}}}{V_s}}\right)^{\frac{1}{3}}} \tag{A.8}$$

$$\frac{\Delta_{sat}}{D_p} = \frac{K_g}{1 - \left(\frac{V_p S}{V_p K_{S_{max}}}\right)^{\frac{1}{3}}} \tag{A.9}$$

Which, dividing through and multiplying up D_p gives:

$$\Delta_{sat} = \frac{K_g D_p}{1 - \left(\frac{S}{K_{S_{max}}}\right)^{\frac{1}{3}}} \tag{A.10}$$

Appendix B. Area of contact derivation

Since

$$Q = p_0 \pi \tilde{R} \delta \tag{B.1}$$

With $\tilde{R}$ being the harmonic mean of the radii The following can be found, δ^* being the final deformation)

$$\int_0^{\delta*} Q d\delta = \frac{p_0 \pi \tilde{R} \delta^{*2}}{2} = E_P \tag{B.2}$$

This then allows the area to be found through the relation

$$Q = p_0 \pi a^2 \tag{B.3}$$

Where a is the radius of the area of contact. Since the force at depth δ^* is

$$Q^* = \pi p_0 \tilde{R} \delta* \tag{B.4}$$

Therefore

$$\delta^* = \frac{Q^*}{p_0 \pi \tilde{R}} \tag{B.5}$$

To find the final force, and hence, the final area of contact:

$$\frac{1}{2} {V_{C_N}}^2 \tilde{m} = \frac{p_0 \pi \tilde{R} \left(\frac{Q^*}{p_0 \pi \tilde{R}}\right)^2}{2} = \frac{Q^{*2}}{2 p_0 \pi \tilde{R}} \tag{B.6}$$

$$Q^* = V_{C_N} \left(\tilde{m} p_0 \pi \tilde{R}\right)^{\frac{1}{2}} = V_{C_N} \sqrt{\widetilde{R R^3}} \sqrt{\frac{4\pi}{3} \rho_g p_0 \pi} \tag{B.7}$$

The harmonic mean of the masses of the particles is separated to get the harmonic mean of the radii cubed, which will be necessary later when determining the limiting diameter. Allowing $p_0 = K_H \sigma_y$, and re-arranging, gives

$$\pi a^{*2} = \pi \sqrt{\frac{4}{3}} \sqrt{\frac{\rho_g}{K_H \sigma_y}} V_{C_N} \sqrt{\widetilde{R R^3}} = A \tag{B.8}$$

Appendix C. Rearrangement of bond limit equation

Putting Eqs. (23) and (26) into (21) gives

$$M = \frac{A_M\left(\rho_g, {V_{ch}}^2, \lambda_{ch}\right)}{2^\alpha} \left(\frac{\hat{D}}{\bar{D}}\right)^{2K_\gamma} \bar{D}^4 = \frac{\frac{K_A \rho_g {V_{ch}}^2}{\lambda_{ch}}}{2^\alpha} \left(\frac{\hat{D}}{\bar{D}}\right)^{2K_\gamma} \bar{D}^4 = \frac{K_\alpha \rho_g {V_{ch}}^2}{\lambda_{ch}} \left(\frac{\hat{D}}{\bar{D}}\right)^{2K_\gamma} \bar{D}^4 \tag{C.1}$$

Substituting Eqs. (28) and (16) into (6) gives:

$$K_{\frac{t}{c}} \sigma_y \alpha_{wet}(\varepsilon_{rr}) > \frac{3 \frac{K_\alpha \rho_g {V_{ch}}^2}{\lambda_{ch}} \left(\frac{\hat{D}}{\bar{D}}\right)^{2K_\gamma} \bar{D}^4}{4\pi^{\frac{3}{2}} \left(\pi \sqrt{\frac{4}{3}} \sqrt{\frac{\rho_g}{K_H \sigma_y}} V_{C_N} \sqrt{\widetilde{R R^3}}\right)^{\frac{3}{2}}} \tag{C.2}$$

expanding this gives

$$K_{\frac{t}{c}} \sigma_y \alpha_{wet}(\varepsilon_{rr}) > \frac{3}{4\pi^{\frac{3}{2}} \left(\sqrt{\frac{4}{3}\pi}\right)^{\frac{3}{2}}} \frac{K_\alpha \rho_g}{\left(\sqrt{\frac{\rho_g}{K_H \sigma_y}}\right)^{\frac{3}{2}}} \frac{\frac{{V_{ch}}^2}{\lambda_{ch}}}{{V_{C_N}}^{\frac{3}{2}}} \left(\frac{\hat{D}}{\bar{D}}\right)^{2K_\gamma} \frac{\bar{D}^4}{\sqrt{\widetilde{R R^3}^3}} \tag{C.3}$$

$$\tilde{R} = \frac{\tilde{D}}{2}, \quad \widetilde{R^3} = \frac{\widetilde{D^3}}{2^3} \tag{C.4}$$

$$K_{\frac{t}{c}} \sigma_y \alpha_{wet}(\varepsilon_{rr}) > \frac{3 * 2^3}{4\pi^{\frac{3}{2}} \left(\sqrt{\frac{4}{3}\pi}\right)^{\frac{3}{2}}} \frac{K_\alpha \rho_g}{\left(\sqrt{\frac{\rho_g}{K_H \sigma_y}}\right)^{\frac{3}{2}}} \frac{\frac{{V_{ch}}^2}{\lambda_{ch}}}{{V_{C_N}}^{\frac{3}{2}}} \left(\frac{\hat{D}}{\bar{D}}\right)^{2K_\gamma} \frac{\bar{D}^4}{\sqrt{\tilde{D}\widetilde{D^3}^3}} \tag{C.5}$$

Arranging with diameters as focus, and noting that

$$\left(\tilde{D}\widetilde{D^3}\right)^{\frac{3}{4}} = \left(\frac{2dD}{(d+D)} \frac{2d^3 D^3}{\left(D^3 + d^3\right)}\right)^{\frac{3}{4}} = \left(\frac{2\hat{D}^2}{2\bar{D}} \frac{2(\hat{D}^2)^3}{2\bar{D^3}}\right)^{\frac{3}{4}} = \left(\frac{\hat{D}^2}{\bar{D}} \frac{\hat{D}^6}{\bar{D^3}}\right)^{\frac{3}{4}} = \frac{\hat{D}^6}{\left(\bar{D}\bar{D^3}\right)^{\frac{3}{4}}} \tag{C.6}$$

$$\left(\frac{\hat{D}}{\bar{D}}\right)^{2K_\gamma} \frac{\bar{D}^4}{\frac{\hat{D}^6}{\left(\bar{D}\bar{D^3}\right)^{\frac{3}{4}}}} < K_{\frac{t}{c}} \sigma_y \alpha_{wet}(\varepsilon_{rr}) \frac{4\pi^{\frac{3}{2}} \left(\sqrt{\frac{4}{3}\pi}\right)^{\frac{3}{2}}}{3 * 2^3} \frac{\left(\sqrt{\frac{\rho_g}{K_H \sigma_y}}\right)^{\frac{3}{2}}}{K_\alpha \rho_g} \frac{\lambda_{ch} {V_{C_N}}^{\frac{3}{2}}}{{V_{ch}}^2} \tag{C.7}$$

Another re-arrangement to get like variables together, and to group the mathematical constants into a single value C_m gives

$$\left(\frac{\hat{D}}{\bar{D}}\right)^{2K_\gamma}\frac{\bar{D}^4\left(\bar{D}\bar{D^3}\right)^{\frac{3}{4}}}{\hat{D}^6} < C_m\frac{K_{\frac{t}{c}}}{K_\alpha K_H^{\frac{3}{4}}}\alpha_{\text{wet}}(\varepsilon_{\text{rr}})\frac{\sigma_y}{\sigma_y^{\frac{3}{4}}}\frac{\rho_g^{\frac{3}{4}}}{\rho_g}\frac{V_{C_N}^{\frac{3}{2}}}{V_{\text{ch}}^2}\lambda_{\text{ch}} \quad \text{(C.8)}$$

Dividing through gives:

$$\left(\frac{\hat{D}}{\bar{D}}\right)^{2K_\gamma-4}\frac{\left(\bar{D}\bar{D^3}\right)^{\frac{3}{4}}}{\hat{D}^2} < C_m\frac{K_{\frac{t}{c}}}{K_\alpha K_H^{\frac{3}{4}}}\alpha_{\text{wet}}(\varepsilon_{\text{rr}})\frac{\sigma_y^{\frac{1}{4}}}{\rho_g^{\frac{1}{4}}}\frac{V_{C_N}^{\frac{3}{2}}}{V_{\text{ch}}^2}\lambda_{\text{ch}} \quad \text{(C.9)}$$

Appendix D. Adjusting for $\mathbf{d = r_d D}$

Allowing $d = r_d D$ gives

$$\bar{D} = \frac{D + r_d D}{2} = \frac{D}{2}(1 + r_d),\ \ \hat{D} = (D r_d D)^{\frac{1}{2}} = D r_d^{\frac{1}{2}} \quad \text{(D.1)}$$

This allows the re-arrangement of the left hand side to form

$$\begin{aligned}&\left(\frac{D r_d^{\frac{1}{2}}}{\frac{D}{2}(1+r_d)}\right)^{2K_\gamma-4}\frac{\left(\frac{D}{2}(1+r_d)\frac{D^3}{2}\left(1+r_d{}^3\right)\right)^{\frac{3}{4}}}{\left(D r_d^{\frac{1}{2}}\right)^2}\\ &= \left(\frac{r_d^{\frac{1}{2}}}{\frac{(1+r_d)}{2}}\right)^{2K_\gamma-4}\frac{\frac{D^3}{2}\left((1+r_d)\left(1+r_d{}^3\right)\right)^{\frac{3}{4}}}{D^2 r_d}\\ &= \frac{\left(1+r_d{}^3\right)^{\frac{3}{4}}}{(1+r_d)^{2K_\gamma-3\frac{1}{4}}}r_d{}^{K_\gamma-3}D = \left(\frac{\left(1+r_d{}^3\right)}{(1+r_d)}\right)^{\frac{3}{4}}\frac{r_d{}^{K_\gamma-3}}{(1+r_d)^{2K_\gamma-4}}D\end{aligned} \quad \text{(D.2)}$$

Finally, since D is the size of the larger of the two granules being merged. The total diameter of the two granules being merged is $D(1+r_d)^{\frac{1}{3}} = \Delta_{\text{bond}}$, so $\frac{\Delta_{\text{bond}}}{(1+r_d)^{\frac{1}{3}}} = D$

$$\left(\frac{\left(1+r_d{}^3\right)}{(1+r_d)}\right)^{\frac{3}{4}}\frac{r_d{}^{K_\gamma-3}}{(1+r_d)^{2K_\gamma-4}}\frac{\Delta_{\text{bond}}}{(1+r_d)^{\frac{1}{3}}} < C_m\frac{K_{\frac{t}{c}}}{K_\alpha K_H^{\frac{3}{4}}}\alpha_{\text{wet}}(\varepsilon_{\text{rr}})\frac{\sigma_y^{\frac{1}{4}}}{\rho_g^{\frac{1}{4}}}\frac{V_{C_N}^{\frac{3}{2}}}{V_{\text{ch}}^2}\lambda_{\text{ch}} \quad \text{(D.3)}$$

$$r_d{}^{K_\gamma-3}\left(1+r_d{}^3\right)^{\frac{3}{4}}\frac{(1+r_d)^{2\frac{11}{12}}}{(1+r_d)^{2K_\gamma}}\Delta_{\text{bond}} < C_m\frac{K_{\frac{t}{c}}}{K_\alpha K_H^{\frac{3}{4}}}\alpha_{\text{wet}}(\varepsilon_{\text{rr}})\frac{\sigma_y^{\frac{1}{4}}}{\rho_g^{\frac{1}{4}}}\frac{V_{C_N}^{\frac{3}{2}}}{V_{\text{ch}}^2}\lambda_{\text{ch}} \quad \text{(D.4)}$$

$$\Delta_{\text{bond}} < C_m\frac{K_{\frac{t}{c}}}{K_\alpha K_H^{\frac{3}{4}}}\alpha_{\text{wet}}(\varepsilon_{\text{rr}})\frac{\sigma_y^{\frac{1}{4}}}{\rho_g^{\frac{1}{4}}}\frac{V_{C_N}^{\frac{3}{2}}}{V_{\text{ch}}^2}\lambda_{\text{ch}}\frac{(1+r_d)^{2K_\gamma-2\frac{11}{12}}}{r_d{}^{K_\gamma-3}\left(1+r_d{}^3\right)^{\frac{3}{4}}} \quad \text{(D.5)}$$

References

[1] S.M. Iveson, J.D. Litster, K. Hapgood, B.J. Ennis, Nucleation, growth and breakage phenomena in agitated wet granulation processes: a review, Powder Technol. 117 (1-2) (2001) 3–39, https://doi.org/10.1016/S0032-5910(01)00313-8.

[2] P.R. Mort, Scale-up of binder agglomeration processes, Powder Technol. 150 (2) (2005) 86–103, https://doi.org/10.1016/j.powtec.2004.11.025.

[3] S. Pohl, P. Kleinebudde, A review of regime maps for granulation, Int. J. Pharm. 587 (2020) 119660, https://doi.org/10.1016/j.ijpharm.2020.119660.

[4] S.M. Iveson, P.A. Wauters, S. Forrest, J.D. Litster, G.M. Meesters, B. Scarlett, Growth regime map for liquid-bound granules: further development and experimental validation, Powder Technol. 117 (1-2) (2001) 83–97, https://doi.org/10.1016/S0032-5910(01)00317-5.

[5] T. Schaefer, P. Holm, H.G. Kristensen, Melt granulation in a laboratory scale high shear mixer, Drug Dev. Ind. Pharm. 16 (8) (1990) 1249–1277, https://doi.org/10.3109/03639049009115960.

[6] M. Ritala, P. Holm, T. Schaefer, H.G. Kristensen, Influence of liquid bonding strength on power consumption during granulation in a high shear mixer, Drug Dev. Ind. Pharm. 14 (8) (1988) 1041–1060, https://doi.org/10.3109/03639048809151919.

[7] D.A. Pohlman, J.D. Litster, Coalescence model for induction growth behavior in high shear granulation, Powder Technol. 270 (PB) (2015) 435–444, https://doi.org/10.1016/j.powtec.2014.07.016.

[8] J.D. Litster, B.J. Ennis, The science and engineering of granulation process, Part. Technol. Ser. 15 (2004) 77, http://link.springer.com/10.1007/978-94-017-0546-2.

[9] P.C. Kapur, D.W. Fuerstenau, Coalescence model for granulation, Indust. Eng. Chem. Proc. Des. Develop. 8 (1) (1969) 56–62, https://doi.org/10.1021/i260029a010.

[10] S. WATANO, Y. SATO, K. MIYANAMI, Scale-up of agitation fluidized bed granulation. IV. scale-up theory based on the kinetic energy similarity. Chem. Pharm. Bull. 43 (7) (1995) 1227–1230, https://doi.org/10.1248/cpb.43.1227.

[11] K.V. Sastry, P. Dontula, C. Hosten, Investigation of the layering mechanism of agglomerate growth during drum pelletization, Powder Technol. 130 (1-3) (2003) 231–237, https://doi.org/10.1016/S0032-5910(02)00271-1.

[12] S.A.L. de Koster, Experimental Investigation and Modelling of Consolidation and Layering Mechanisms in High-Shear Granulation, 2018 http://etheses.whiterose.ac.uk/21234/.

[13] P.C. Kapur, V. Runkana, Balling and granulation kinetics revisited, Int. J. Miner. Process. 72 (1-4) (2003) 417–427, https://doi.org/10.1016/S0301-7516(03)00116-9.

[14] P. Holm, T. Schaefer, H.G. Kristensen, Granulation in high-speed mixers Part V. Power consumption and temperature changes during granulation, Powder Technol. 43 (3) (1985) 213–223, https://doi.org/10.1016/0032-5910(85)80002-4.

[15] J.B. Wade, G.P. Martin, D.F. Long, Feasibility assessment for a novel reverse-phase wet granulation process: the effect of liquid saturation and binder liquid viscosity, Int. J. Pharm. 475 (1) (2014) 450–461, https://doi.org/10.1016/j.ijpharm.2014.09.012.

[16] H.G. Kristensen, P. Holm, T. Schaefer, Mechanical properties of moist agglomerates in relation to granulation mechanisms part II. Effects of particle size distribution, Powder Technol. 44 (3) (1985) 239–247, https://doi.org/10.1016/0032-5910(85)85005-1.

[17] T. Schaefer, P. Holm, H.G. Kristensen, Wet granulation in a laboratory scale high shear mixer, Pharmazeutische Indust. 52 (9) (1990) 1147–1153.

[18] S.T. Keningley, P.C. Knight, A.D. Marson, An investigation into the effects of binder viscosity on agglomeration behaviour, Powder Technol. 91 (2) (1997) 95–103, https://doi.org/10.1016/S0032-5910(96)03230-5.

[19] P.K. Le, P. Avontuur, M.J. Hounslow, A.D. Salman, The kinetics of the granulation process: right from the early stages, Powder Technol. 189 (2) (2009) 149–157, https://doi.org/10.1016/j.powtec.2008.04.018.

[20] F. Hoornaert, P.A. Wauters, G.M. Meesters, S.E. Pratsinis, B. Scarlett, Agglomeration behaviour of powders in a Lodige mixer granulator, Powder Technol. 96 (2) (1998) 116–128, https://doi.org/10.1016/S0032-5910(97)03364-0.

[21] P.A. Wauters, R. Van de Water, J.D. Litster, G.M. Meesters, B. Scarlett, Growth and compaction behaviour of copper concentrate granules in a rotating drum, Powder Technol. 124 (3) (2002) 230–237, https://doi.org/10.1016/S0032-5910(02)00029-3.

[22] A.C. Santomaso, R. Baggio, F. Zorzi, G. Salviulo, N. Realdon, E. Franceschinis, Sugars with different thickening power in high shear granulation, Powder Technol. 317 (2017) 391–399, https://doi.org/10.1016/j.powtec.2017.05.017.

[23] B.J. Ennis, G. Tardos, R. Pfeffer, A microlevel-based characterization of granulation phenomena, Powder Technol. 65 (1-3) (1991) 257–272, https://doi.org/10.1016/0032-5910(91)80189-P.

[24] L.X. Liu, J.D. Litster, S.M. Iveson, B.J. Ennis, Coalescence of deformable granules in wet granulation processes, AIChE J. 46 (3) (2000) 529–539, https://doi.org/10.1002/aic.690460312.

[25] L.X. Liu, J.D. Litster, Population balance modelling of granulation with a physically based coalescence kernel, Chem. Eng. Sci. 57 (2002) 2183–2191 www.elsevier.com/locate/ces.

[26] S.M. Iveson, J.D. Litster, Growth regime map for liquid-bound granules, AIChE J. 44 (7) (1998) 1510–1518, https://doi.org/10.1002/aic.690440705.

[27] S.M. Iveson, J.D. Litster, Liquid-bound granule impact deformation and coefficient of restitution, Powder Technol. 99 (3) (1998) 234–242, https://doi.org/10.1016/S0032-5910(98)00115-6.

[28] A.A. Adetayo, J.D. Litster, S.E. Pratsinis, B.J. Ennis, Population balance modelling of drum granulation of materials with wide size distribution, Powder Technol. 82 (1) (1995) 37–49, https://doi.org/10.1016/0032-5910(94)02896-V.

[29] J. Shabanian, M.A. Duchesne, A. Runstedtler, M. Syamlal, R.W. Hughes, Improved analytical energy balance model for evaluating agglomeration from a binary collision of identical wet particles, Chem. Eng. Sci. 223 (2020) 115738, https://doi.org/10.1016/j.ces.2020.115738.

[30] M. Butensky, D. Hyman, Rotary drum granulation. An experimental study of the factors affecting granule size, Ind. Eng. Chem. Fundam. 10 (2) (1971) 212–219, https://doi.org/10.1021/i160038a005.

[31] M.E.D. Urso, C.J. Lawrence, M.J. Adams, Pendular, funicular, and capillary bridges: results for two dimensions, J. Colloid Interface Sci. 220 (1) (1999) 42–56, https://doi.org/10.1006/jcis.1999.6512.

[32] M. Scheel, R. Seemann, M. Brinkmann, M. Di Michiel, A. Sheppard, B. Breidenbach, S. Herminghaus, Morphological clues to wet granular pilestability, Nat. Mater. 7 (3) (2008) 189–193, https://doi.org/10.1038/nmat2117.

[33] N. Ouchiyama, T. Tanaka, The probability of coalescence in granulation kinetics, Indust. Eng. Chem. Proc. Des. Develop. 14 (3) (1975) 286–289, https://doi.org/10.1021/i260055a016.

[34] S. Iveson, N. Page, Tensile bond strength development between liquid-bound pellets during compression, Powder Technol. 117 (1-2) (2001) 113–122, https://doi.org/10.1016/S0032-5910(01)00319-9.

[35] S.M. Iveson, J.A. Beathe, N.W. Page, The dynamic strength of partially saturated powder compacts: the effect of liquid properties, Powder Technol. 127 (2) (2002) 149–161, https://doi.org/10.1016/S0032-5910(02)00118-3.

[36] M.R. Brake, An analytical elastic-perfectly plastic contact model, Int. J. Solids Struct. 49 (22) (2012) 3129–3141, https://doi.org/10.1016/j.ijsolstr.2012.06.013.

[37] S. Kumar, C. Toan, Vahedifard, poisson's ratio characteristic curve of unsaturated soils, J. Geotech. Geoenviron. Eng. 147 (2021) 04020149, https://doi.org/10.1061/(ASCE)GT. 1943-5606.0002424.
[38] J. Jamari, D.J. Schipper, Experimental investigation of fully plastic contact of a sphere against a hard flat, J. Tribol. 128 (2) (2006) 230–235, https://doi.org/10.1115/1.2164470.
[39] M. Adepu, S. Hate, A. Bétard, S. Oka, M. Schongut, M. Sen, Y. Sood, D. Wolf, S. Wieland, F. Stepanek, F. Muzzio, B. Glasser, R. Ramachandran, Quantitative validation and analysis of the regime map approach for the wet granulation of industrially relevant zirconium hydroxide powders, Powder Technol. 294 (2016) 177–184, https://doi.org/10.1016/j.powtec.2016.02.026.
[40] K.L. Johnson, K. Kendall, A.D. Roberts, Surface energy and the contact of elastic solids, Proceed. Royal Soc. Lon. A. Mathemat. Phys. Sci. 324 (1558) (1971) 301–313, https://doi.org/10.1098/rspa.1971.0141.
[41] E. Barthel, Adhesive elastic contacts - JKR and more, J. Phys. D: Appl. Phys. 41 (2008) 163001, https://doi.org/10.1088/0022-3727/41/16/163001.
[42] I. Goldhirsch, Introduction to granular temperature, Powder Technol. 182 (2) (2008) 130–136, https://doi.org/10.1016/j.powtec.2007.12.002.
[43] M.J. Hounslow, J.M. Pearson, T. Instone, Tracer studies of high-shear granulation: II. population balance modeling, AIChE J. 47 (9) (2001) 1984–1999, https://doi.org/10.1002/aic.690470910.
[44] G.I. Tardos, M.I. Khan, P.R. Mort, Critical parameters and limiting conditions in binder granulation of fine powders, Powder Technol. 94 (3) (1997) 245–258, https://doi.org/10.1016/S0032-5910(97)03321-4.
[45] L.X. Liu, R. Smith, J.D. Litster, Wet granule breakage in a breakage only high-hear mixer: effect of formulation properties on breakage behaviour, Powder Technol. 189 (2) (2009) 158–164, https://doi.org/10.1016/j.powtec.2008.04.029.
[46] H. Rumpf, H. Schubert, The behavior of agglomerates under tensile strain, J. Chem. Eng. Jpn. 7 (4) (1974) 294–298, https://doi.org/10.1252/jcej.7.294.
[47] K. Van Den Dries, H. Vromans, Relationship between inhomogeneity phenomena and granule growth mechanisms in a high-shear mixer, Int. J. Pharm. 247 (1-2) (2002) 167–177, https://doi.org/10.1016/S0378-5173(02)00419-2.
[48] H. Schubert, W. Herrmann, H. Rumpf, Deformation behaviour of agglomerates under tensile stress, Powder Technol. 11 (2) (1975) 121–131, https://doi.org/10.1016/0032-5910(75)80037-4.
[49] H. Louati, D. Oulahna, A. de Ryck, A.D. Ryck, Effect of the particle size and the liquid content on the shear behaviour of wet granular material, Powder Technol. 315 (2017) 398–409, https://doi.org/10.1016/j.powtec.2017.04.030.
[50] P.A. Wauters, R.B. Jakobsen, J.D. Litster, G.M. Meesters, B. Scarlett, Liquid distribution as a means to describing the granule growth mechanism, Powder Technol. 123 (2-3) (2002) 166–177, https://doi.org/10.1016/S0032-5910(01)00446-6.
[51] S.M. Iveson, J.D. Litster, B.J. Ennis, Fundamental studies of granule consolidation part 1: effects of binder content and binder viscosity, Powder Technol. 88 (1) (1996) 15–20, https://doi.org/10.1016/0032-5910(96)03096-3.
[52] S.M. Iveson, J.D. Litster, Fundamental studies of granule consolidation. Part 2: Quant. Effect Part. Binder Proper. Powder Tech. 99 (3) (1998) 243–250, https://doi.org/10.1016/S0032-5910(98)00116-8.
[53] S. WATANO, Y. SATO, K. MIYANAMI, T. MURAKAMI, N. NAGAMI, Y. ITO, T. KAMATA, N. ODA, Scale-up of agitation fluidized bed granulation. II. Effects of scale, air flow velocity and agitator rotational speed on granule size, size distribution, density and shape, Chem. Pharm. Bull. 43 (7) (1995) 1217–1220, https://doi.org/10.1248/cpb.43.1217.
[54] glossary of terms used in chemical kinetics, including reaction dynamics (iupac recommendations 1996), Pure Appl. Chem. 68 (1) (1996) 149–192, https://doi.org/10.1351/pac199668010149.
[55] J.B. Wade, G.P. Martin, D.F. Long, The development of a growth regime map for a novel reverse-phase wet granulation process, Int. J. Pharm. 512 (1) (2016) 224–233, https://doi.org/10.1016/j.ijpharm.2016.08.050.
[56] M. Nicodemi, Dynamical response functions in models of vibrated granular media, Phys. Rev. Lett. 82 (19) (1999) 3734–3737, https://doi.org/10.1103/PhysRevLett.82.3734.
[57] L.A. Pugnaloni, I. Sánchez, P.A. Gago, J. Damas, I. Zuriguel, D. Maza, Towards a relevant set of state variables to describe static granular packings, physical review E - statistical, Nonlinear Soft Mat. Phys. 82 (5) (2010) 1–4, https://doi.org/10.1103/PhysRevE.82.050301.
[58] M.I. Khan, G.I. Tardos, Stability of wet agglomerates in granular shear flows, J. Fluid Mech. 347 (1997) 347–368, https://doi.org/10.1017/S002211209700668X.
[59] A.Z.A.A. Hassn, Mutli-Stage Granulation in a High Shear Mixer (November), 2018.
[60] M. B”orner, M. Michaelis, E. Siegmann, C. Radeke, U. Schmidt, Impact of impeller design on high-shear wet granulation, Powder Technol. 295 (2016) 261–271, https://doi.org/10.1016/j.powtec.2016.03.023.
[61] H. Nakamura, H. Fujii, S. Watano, Scale-up of high shear mixer-granulator based on discrete element analysis, Powder Technol. 236 (2013) 149–156, https://doi.org/10.1016/j.powtec.2012.03.009.
[62] D.M. Newitt, J.M. Conway-Jones, A Contribution to the Theory and Practice of Granulation, 1958.
[63] S. Bellinghausen, E. Gavi, L. Jerke, P.K. Ghosh, A.D. Salman, J.D. Litster, Nuclei size distribution modelling in wet granulation, Chem. Eng. Sci.: X 4 (2019) 100038, https://doi.org/10.1016/j.cesx.2019.100038.
[64] K.P. Hapgood, J.D. Litster, R. Smith, Nucleation regime map for liquid bound granules, AIChE J. 49 (2) (2003) 350–361, https://doi.org/10.1002/aic.690490207.
[65] B. Waldie, Growth mechanism and the dependence of granule size on drop size in fluidized-bed granulation, Chem. Eng. Sci. 46 (11) (1991) 2781–2785, https://doi.org/10.1016/0009-2509(91)85147-P.
[66] S.L. Rough, D.I. Wilson, D.W. York, Effect of solids formulation on the manufacture of high shear mixer agglomerates, Adv. Powder Technol. 16 (2) (2005) 145–169, https://doi.org/10.1163/1568552053621704.
[67] R.M. Smith, L.X. Liu, J.D. Litster, Breakage of drop nucleated granules in a breakage only high shear mixer, Chem. Eng. Sci. 65 (21) (2010) 5651–5657, https://doi.org/10.1016/j.ces.2010.06.037.
[68] M.J. Hounslow, M. Oullion, G.K. Reynolds, Kinetic models for granule nucleation by the immersion mechanism, Powder Technol. 189 (2) (2009) 177–189, https://doi.org/10.1016/j.powtec.2008.04.008.
[69] T. Hao, Defining temperatures of granular powders analogously with thermodynamics to understand jamming phenomena, AIMS Mat. Sci. 5 (1) (2018) 1–33, https://doi.org/10.3934/matersci.2018.1.1.